Liu, Suhong; Afan, Haitham Abdulmohsin; Aldlemy, Mohammed Suleman; Al-Ansari, Nadhir; Yaseen, Zaher Mundher

**Article**

# Energy analysis using carbon and metallic oxides-based nanomaterials inside a solar collector

Energy Reports

**Provided in Cooperation with:**
Elsevier

*Suggested Citation:* Liu, Suhong; Afan, Haitham Abdulmohsin; Aldlemy, Mohammed Suleman; Al-Ansari, Nadhir; Yaseen, Zaher Mundher (2020) : Energy analysis using carbon and metallic oxides-based nanomaterials inside a solar collector, Energy Reports, ISSN 2352-4847, Elsevier, Amsterdam, Vol. 6, pp. 1373-1381, https://doi.org/10.1016/j.egyr.2020.05.015

This Version is available at:
https://hdl.handle.net/10419/244127

Energy Reports 6 (2020) 1373–1381

Contents lists available at ScienceDirect

Energy Reports

journal homepage: www.elsevier.com/locate/egyr

Research paper

# Energy analysis using carbon and metallic oxides-based nanomaterials inside a solar collector

Suhong Liu [a], Haitham Abdulmohsin Afan [b], Mohammed Suleman Aldlemy [c], Nadhir Al-Ansari [d], Zaher Mundher Yaseen [e,*]

[a] School of Mathematics and Information Science, Baoji University of Arts and Sciences, 721000, Shaanxi, China
[b] Institute of Research and Development, Duy Tan University, Da Nang 550000, Viet Nam
[c] Department of Mechanical Engineering, Collage of Mechanical Engineering Technology, Benghazi-Libya
[d] Civil, Environmental and Natural Resources Engineering, Lulea University of Technology, 97187 Lulea, Sweden
[e] Sustainable Developments in Civil Engineering Research Group, Faculty of Civil Engineering, Ton Duc Thang University, Ho Chi Minh City, Viet Nam

ARTICLE INFO

*Article history:*
Received 26 December 2019
Received in revised form 16 May 2020
Accepted 19 May 2020
Available online 26 May 2020

*Keywords:*
Flat plate solar collector
Thermal efficiency
Graphene
Graphene nanoplatelets
Metallic oxides

ABSTRACT

The effectiveness of a flat-plate solar collector was studied by using $SiO_2$, $Al_2O_3$, Graphene, and graphene nanoplatelets nanofluids with distilled water as the working fluids. The energy efficiency was theoretically compared using MATLAB programming. The prepared carbon and metallic oxides nanomaterials were structurally and morphologically characterized via field emission scanning electron microscope. The study was conducted under different operating conditions such as different volume fractions (0.25%, 0.5%, 0.75% and 1%), fluid mass flow rate (0.0085, 0.017, and 0.0255 kg/s), input temperatures (30, 40, and 50 °C), and solar irradiance (500, 750, and 1000 W/m$^2$). Nanofluids showed better thermophysical properties compared to standard working fluids. With the addition of the nanofluids $SiO_2$, $Al_2O_3$, Gr and GNPs to the FPSC the highest efficiency of 64.45%, 67.03%, 72.45%, and 76.56% respectively was reached. The results suggested that nanofluids made from carbon nanostructures and metallic oxides can be used in solar collectors to increase the parameters of heat absorbed/loss compared to water only usage.



## 1. Introduction

A flat-plate solar collector (FPSC) is among the main types of solar collectors that form the major active components of heating systems (Kong et al., 2015; Mallah et al., 2019). In addition to FPSC, the other major types of solar collectors are integrated collector-storage systems and evacuated tube collectors (Kabeel et al., 2016). An FPSC is made up of a metal box (insulated on its backside) with glazing. Sun rays are absorbed by the plate and transferred to a circulating fluid which flows in the collector pipes (Li et al., 2017; Raj and Subudhi, 2018).

Among the trending approaches towards improving the effectiveness of FPSC, nanofluids were employed as heat transfer agents rather than using regular fluids. Originally, Choi and Eastman (Choi and Eastman, 1995) described the "nanofluid" as a combination of base fluid and nanomaterials (with size < 100-nm). These exhibited superior thermophysical properties, allowing a heat transfer and a heat absorption more effective than with typical liquids (Azmi et al., 2016; Gupta et al., 2017; Zayed et al., 2019). For a broad domain of solar collectors, many types of nanofluids were used (Borode et al., 2019; Farhana et al., 2019; Sarsam et al., 2015). Faizal et al. (2013) developed a smaller solar collector for different nanofluids to calculate cost-saving, performance, size reduction and embodied energy saving. The study as mentioned earlier estimated that a maximum weight of 10,239 kg, 8625 kg, 8857 kg could be saved for CuO-$H_2O$, $SiO_2$-$H_2O$, $TiO_2$-$H_2O$ and $Al_2O_3$-$H_2O$ for 1000 solar collector devices, respectively. Theoretically, Alim et al. (2013) used different nanofluids ($Al_2O_3$-$H_2O$, $SiO_2$-$H_2O$, CuO-$H_2O$, $TiO_2$-$H_2O$) to test improvement in heat transfer, entropy generation, and pressure loss within an FPSC. In a theoretical study of (Mahian et al., 2014), the quality of the mini channel-based solar plate collector was evaluated, including Cu-$H_2O$, $Al_2O_3$-$H_2O$, $TiO_2$-$H_2O$, and $SiO_2$-$H_2O$, four types of nanofluids were used. Results showed that $Al_2O_3$-$H_2O$ nanofluid experienced the highest increase in heat transfer, while $SiO_2$-$H_2O$ nanofluid recorded the lowest rise. Both the efficiency and total annual cost were studied in different volumetric fractions at different types of nanoparticles containing $Al_2O_3$, $SiO_2$, and CuO (Hajabdollahi et al., 2019). When $Al_2O_3$-$H_2O$, $SiO_2$-$H_2O$, and CuO-$H_2O$ were tested, the output improved by 4.47%, 4.65%, and 5.22% relative to base fluid with a total annual

* Corresponding author.
*E-mail addresses:* leidou0315@qq.com (S. Liu), haithamabdulmohsinafan@duytan.edu.vn (H.A. Afan), maldlemy@ceb.edu.ly (M.S. Aldlemy), nadhir.alansari@ltu.se (N. Al-Ansari), yaseen@tdtu.edu.vn (Z.M. Yaseen).

https://doi.org/10.1016/j.egyr.2020.05.015

**Table 1**
The density and specific heat capacity of $Al_2O_3$, $SiO_2$, GNPs, and Gr nanofluids at different volume concentrations and temperatures.

| | $Al_2O_3$-DW | | | | | | | | | | | |
|---|---|---|---|---|---|---|---|---|---|---|---|---|
| | 30 °C | | | | 40 °C | | | | 50 °C | | | |
| | 0.25% | 0.5% | 0.75% | 1% | 0.25% | 0.5% | 0.75% | 1% | 0.25% | 0.5% | 0.75% | 1% |
| $\rho$ (kg/m$^3$) | 1003 | 1010 | 1017 | 1025 | 999 | 1007 | 1014 | 1022 | 995 | 1003 | 1010 | 1018 |
| $C_p$ (J/kg K) | 4037 | 4005 | 3973 | 3942 | 4034 | 4002 | 3970 | 3939 | 4033 | 4001 | 3969 | 3937 |
| | $SiO_2$-DW | | | | | | | | | | | |
| | 30 °C | | | | 40 °C | | | | 50 °C | | | |
| | 0.25% | 0.5% | 0.75% | 1% | 0.25% | 0.5% | 0.75% | 1% | 0.25% | 0.5% | 0.75% | 1% |
| $\rho$ (kg/m$^3$) | 998 | 1001 | 1004 | 1007 | 995 | 998 | 1001 | 1004 | 991 | 994 | 997 | 1000 |
| $C_p$ (J/kg K) | 4052 | 4033 | 4015 | 3997 | 4049 | 4030 | 4012 | 3994 | 4047 | 4029 | 4010 | 3992 |
| | GNPs-DW | | | | | | | | | | | |
| | 30 °C | | | | 40 °C | | | | 50 °C | | | |
| | 0.25% | 0.5% | 0.75% | 1% | 0.25% | 0.5% | 0.75% | 1% | 0.25% | 0.5% | 0.75% | 1% |
| $\rho$ (kg/m$^3$) | 998 | 1001 | 1003 | 1006 | 995 | 997 | 1000 | 1003 | 990 | 993 | 996 | 999 |
| $C_p$ (J/kg K) | 4055 | 4040 | 4025 | 4010 | 4052 | 4037 | 4022 | 4007 | 4051 | 4036 | 4021 | 4006 |
| | Gr-DW | | | | | | | | | | | |
| | 30 °C | | | | 40 °C | | | | 50 °C | | | |
| | 0.25% | 0.5% | 0.75% | 1% | 0.25% | 0.5% | 0.75% | 1% | 0.25% | 0.5% | 0.75% | 1% |
| $\rho$ (kg/m$^3$) | 998 | 1001 | 1004 | 1007 | 995 | 998 | 1001 | 1004 | 991 | 994 | 997 | 1000 |
| $C_p$ (J/kg K) | 4052 | 4034 | 4016 | 3999 | 4049 | 4031 | 4013 | 3995 | 4048 | 4030 | 4012 | 3994 |

cost of $67. With a fixed efficiency of 0.564, the total yearly cost fell by 25.45%, 25.87% and 27.88%, respectively.

Carbon allotropes were studied as absorbing media rather than commercial nanomaterials within the FPSCs such as SWCNT, MWCNTs, graphene (Gr), graphene nanoplatelets (GNPs), and graphene oxide (GO) (Sadripour, 2017; Said et al., 2015; Vakili et al., 2016; Vincely and Natarajan, 2016). Experimental and theoretical investigations were conducted by (Said et al., 2015, 2014) to test the pressure drop, heat transfer, energy and exergy efficiencies of SWCNT-$H_2O$ for (3 wt% and 0.5 kg/min) inside a solar collector system. The tests revealed that the energetic efficiency reached almost 95% while the exergetic efficiency reached 26.25%. The solar energy efficiency was found to be improved by 28.6% for 0.2 wt.%-MWCNT-DW at a mass flow rate of 2 kg/min (Yousefi et al., 2012). Vakili et al. (2016) revealed that at a flow rate of 0.9 kg/min, the improvements in the energy effectiveness were up to 13.5%, 19.7% and 23.2% for 0.0005 wt.%-, 0.001 wt.%- and 0.005 wt.%-GNP nanofluids, respectively. The theoretical and experimental tests of Ahmadi et al. (2016) showed an enhancement in the collector energy by 18.9% with 0.02 wt.%-Gr-$H_2O$ at 0.9 kg/min. Verma et al. (2017) discussed the effects of employing various nanofluids such as MWCNT, GNPs, CuO, $Al_2O_3$, $TiO_2$, and $SiO_2$ on the thermal efficiency of a solar collector. The data showed the use of MWCNTs and GNPs improve thermal performance by 23.47% and 16.97%, respectively. Moreover, experimental data exhibited the maximum improvement of 18.2% in energy efficiency relative to the base fluid under the same conditions for using 0.1 wt.%-CGNP-$H_2O$ nanofluid in the solar collector at 0.0260 kg/s m$^2$-flow rate (Akram et al., 2019). Recently, graphene nanoplatelets were covalently functionalized to use them as absorbing mediums inside the indoor solar collector system (Alawi et al., 2019a,b,c). The experimental and theoretical analyses showed an increase of 10.7%, 11.1%, and 13.3% in the thermal performance for 0.00833, 0.01667, and 0.025 kg/s-GNP-PEG-$H_2O$, respectively.

In the current research, MATLAB programming software was developed for the estimation process of the solar collector thermal efficiency coefficients. Hence, a comparative study was conducted in the research on the use of different heat transfer fluids to the solar collector. Graphene nanoplatelets, graphene, alumina and silica were prepared to analyze the FPSC-efficiency with different volume fractions, mass flow rates, heat supply rates, and input temperatures. The study was performed theoretically using a MATLAB code based on the testing data.

## 2. Materials and methods

### 2.1. Preparation and characterization of nanofluids

In this research for different volume fractions of GNPs, Gr, $Al_2O_3$, and $SiO_2$ nanofluids were used as working fluids to test the thermal performance of FPSC. The chemical procedure of making GNPs and Gr was adopted from Alawi et al. (2018) and Alawi et al. (2019a,b,c). Furthermore, the dry Aluminum oxide and silicon dioxide in the size of (50 nm) were obtained from Sigma-Aldrich. The density and specific heat capacity measurements for the solid nanoparticles were conducted using a density meter (Mettler Toledo DM40) and a differential scanning calorimeter (TA Instruments Q2000), respectively. The density and specific heat of the distilled water were collected from the "National Institute of Standards and Technology (NIST)". The specific heat and density of the different samples were obtained using the equations of (Pak and Cho, 1998). The properties of the nanofluids for different volume concentrations and different temperatures are given in Table 1. In this research, the characterization of the synthesized doped and un-doped powders in terms of their morphology and particle size was done via "Field Emission Scanning Electron Microscopy".

### 2.2. Energy analysis of solar collector

The theoretical model was developed based on the specifications of FPSC as listed in Table 2. The overall heat loss from the solar collector comprises those from the glass plate, from back and edge insulation. It is assumed that all losses are dependent on the same mean plate temperature $T_{pm}$, the collector's total heat loss can be obtained as (Duffie and Beckman, 2013; Kalogirou, 2013):

$$Q_{loss} = U_L A_c \left(T_{pm} - T_a\right) \quad (1)$$

where: $U_L$ —describes to the overall heat loss coefficient. $A_c$ refers to the area of the collector while ($T_{pm}$-$T_a$) is the difference between the mean plate and ambient temperatures.

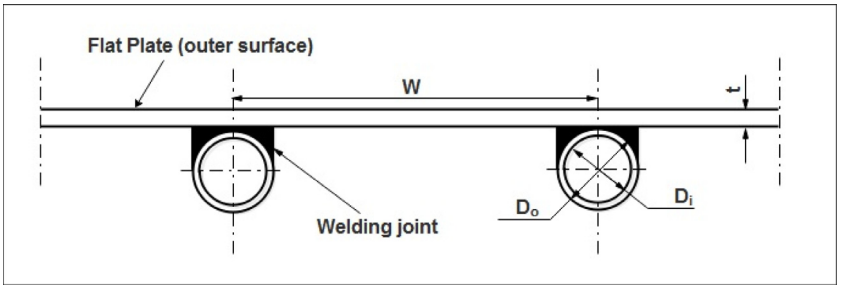


**Fig. 1.** Schematic of a flat sheet and tube absorber.

The total heat loss is the summation of all the heat losses through the top, back, and edge insulation:

$$Q_{loss} = Q_t + Q_b + Q_e \tag{2}$$

where $t$, $b$, and $e$ are the top, back, and edge, respectively.

To estimate the top collector-to-environment loss coefficient ($U_t$), an empirical equation to be utilized for both manual and computer calculations (Duffie and Beckman, 2013):

$$U_t = \left| \frac{N}{\frac{cc}{T_{pm}}\left[\frac{(T_{pm}-T_a)}{N-ff}\right]^{ee}} + \frac{1}{h_{wind}} \right|^{-1} + \frac{\sigma\left(T_{pm}-T_a\right)*\left(T_{pm}^2+T_a^2\right)}{\frac{1}{\varepsilon_p+0.00591Nh_{wind}} + \frac{2N+ff-1+0.133\varepsilon_p}{\varepsilon_g} - N} \tag{3}$$

where, $ff = (1 - 0.089h_{\text{wind}} + 0.1166h^2{}_{\text{wind}}\varepsilon_{\text{p}})(1 + 0.078661N)$

$CC = 520(1 - 0.000051\varphi^2)$

$ee = 0.430(1 - 100/T_{\text{pm}})$

$T_{pm}$ Mean temperature of the absorber plate

($N$, $\sigma$, $\varepsilon_g$, $\varepsilon_{ap}$, $h_{wind}$, $\varphi$) are the number of glasses, Stefan–Boltzmann constant, the emittance of glass, emittance of the absorber plate, wind-heat transfer coefficient and the nanoparticle concentration, respectively.

The following formula was used to estimate the back-heat loss ($Q_b$) (Duffie and Beckman, 2013; Kalogirou, 2013):

$$Q_b = \frac{k_b}{L_b} A_c \left(T_{pm} - T_a\right) \tag{4}$$

where $L_b$ is the thickness of back insulation and $k_b$ is its thermal conductivity.

The estimation of the edge losses can be done by assuming one-dimensional sidewall heat flow through the solar collector's perimeter:

$$Q_e = \frac{k_e}{L_e} A_e \left(T_{pm} - T_a\right) \tag{5}$$

where $k_e$ is the thermal conductivity of edge insulation and $L_e$ is its thickness; while $A_e$ is the edge area of the collector.

Eq. (6) can be used to derive useful heat from the solar collector (Tong et al., 2019).

$$Q_u = \dot{m} C_p \left(T_o - T_i\right) \tag{6}$$

where $\dot{m}$ is the fluid mass flow rate, $C_p$ refers to the specific heat and ($T_o$-$T_i$) is the difference between output and input temperatures.

Also, it is possible to obtain the nanofluids' specific heat and density using Eqs. (7), (8) (Sundar and Sharma, 2008; Tong et al., 2019).

$$C_{p_{nf}} = \frac{(1-\varphi)\rho_{bf} C_{p_{bf}} + \varphi \rho_{np} C_{p_{np}}}{(1-\varphi)\rho_{bf} + \varphi \rho_{np}} \tag{7}$$

$$\rho_{nf} = (1-\varphi)\rho_{bf} + \varphi \rho_{np} \tag{8}$$

where the subscripts of ($nf$, $bf$ and $np$) refer to nanofluid, base fluid and nanoparticles.

Through Eqs. (9)–(10), the energy efficiency of the solar collector can be derived using the useful heat and specific heat of the nanosuspensions (Amin et al., 2015; Mahian et al., 2014).

$$\eta_{th} = \frac{Q_u}{A_C G_T} = \frac{\dot{m} C_p \left(T_o - T_i\right)}{A_C G_T} \tag{9}$$

$$\eta_{th} = F_R(\tau\alpha) - F_R U_L \frac{T_i - T_a}{G_T} \tag{10}$$

where $\eta_{th}$-the thermal efficiency, $Q_{\text{u}}$: the heat gain, $A_{\text{c}}$: the area of the collector, $G_T$: total solar irradiance, $\dot{m}$: the mass flow rate, $C_{\text{p}}$: the specific heat, ($T_o$-$T_i$): the difference between the outlet/inlet temperatures, ($T_i$-$T_a$): the difference between the inlet/ambient temperatures, $U_L$ — the total loss coefficient, $F_{\text{R}}(\tau\alpha)$ — the heat absorption parameter ($F_{\text{R}}U_{\text{L}}$) — the heat removal parameter.

The collector-fin efficiency factor ($\acute{\text{F}}$) is the ratio between the real heat gain to the energy gain under the ideal condition of ($T_{fin} = T_{local-fluid}$). This ratio can be expressed as the ratio between the thermal resistance of (collector-environment) to the thermal resistance of (fluid-environment). In this regard, ($\acute{\text{F}}$) demonstrates the relationship for the fin-riser pipe part within the solar collector system. Fig. 1 displays the schematic diagram of the flat-plate sheet and tube configuration. The collector-fin showed in Fig. 1 with a length of ((*W-D)/2*), an elemental region of width ($dx$) and unit length in the flow direction.

The absorption of solar radiation by the working liquid via the absorber allows an increase in the fluids' temperature. From the efficiency factor of the collector and its flow factor, as shown in Eqs. (12)–(13), Eq. (11) indicates the heat removal factor ($F_{\text{R}}$): (Amin et al., 2015; Mahian et al., 2014).

$$F_R = F' F'' \tag{11}$$

$$F' = \frac{{}^{1}/_{U_L}}{W\left[\frac{1}{U_L[D+(W-D)F]} + \frac{1}{C_b} + \frac{1}{\pi D_i h_{fi}}\right]} \tag{12}$$

$$F'' = \frac{\dot{m} C_p}{A_C U_L F'}\left[1 - exp\left(\frac{-A_c U_L F'}{\dot{m} C_p}\right)\right] \tag{13}$$

where $W$ — the space between two parallel tubes, $D$ — the tubes' outer diameter, $D_{\text{i}}$ — the tubes' inner diameter. $C_b$ — the conductance of the bond which can be estimated according to (Amin et al., 2015; Mahian et al., 2014).

$$C_b = \frac{k_b b}{\gamma} \tag{14}$$

where $k_b$ — the heat conductivity of the bond, $\gamma$ — the average thickness of the bond, and $b$ — the width of the bond.

Therefore, term $F$ denotes the fin efficiency and can be found via Eq. (15) (Amin et al., 2015; Mahian et al., 2014).

$$F = \frac{tanh\left[m\left(W-D\right)/2\right]}{m\left(W-D\right)/2} \tag{15}$$

**Table 2**
Technical specifications of the FPSC setup.

| Details of parameters | Specification |
|---|---|
| Collector area | 3 $m^2$ |
| Absorber plate thickness | 0.6 mm |
| Absorber plate thermal conductivity | 385 W/m K |
| Absorber plate solar absorption | 0.95 |
| Transmissivity of glass sheet | 0.95 |
| Inner and outer diameter of pipes | 10 mm, 11 mm |
| Tube spacing | 0.15 m |
| Bond conductance | 385 W/m K |
| Ambient temperature | 18 °C |

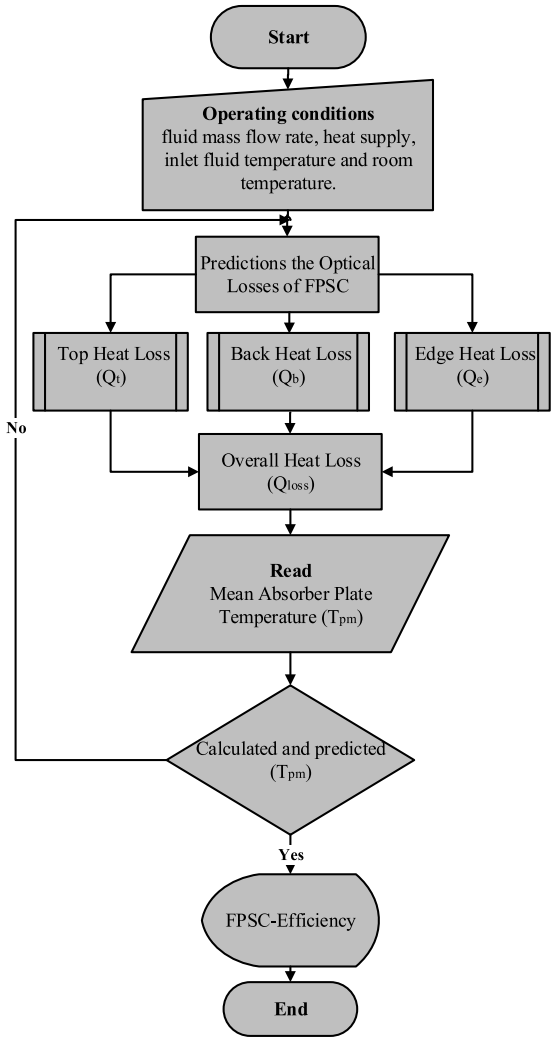


**Fig. 2.** The programming flowchart adopted using MATLAB software.

$$m = \sqrt{\frac{U_L}{k\delta}} \tag{16}$$

To solve the mathematical model and perform the simulation in this study, a MATLAB program was developed using the above analysis. A collector's energy efficiency using nanofluids was modeled with some modifications following the Hottel–Whillier (HW) mathematical model initially developed by (Duffie and Beckman, 2013). Fig. 2 displays the flowchart for this MATLAB process.

## 3. Results and discussion

### 3.1. Morphological analysis of nanofluids

The FESEM images of the prepared GNPs, as shown in Fig. 3(a), exhibit numerous GNP flakes of varying diameters, signifying the absence of impurities in the samples. The majority of the flakes appear transparent on the electron beam, meaning that the layers thickness is limited. Notwithstanding the inability to determine the accurate flakes and defects diameter via FESEM, the planar morphology of GNP layers was more pronounced on the obtained FESEM images. The FESEM images of the prepared Gr, as obtained via high-resolution imaging without any form of pre-treatment due to the materials' high conductivity, are shown in Fig. 3(b). Fig. 3(b) exhibits the intactness and uniformity across the grains. Another observation is that the strict functionalization process caused the observed curvatures and crumpling on some of the transparent FESEM images via the electron beam. Some of the Gr images exhibit the wrinkles associated with functionalization due to the attachment of new functional groups.

The acquired FESEM image of $Al_2O_3$-$H_2O$ nanofluid, as shown in Fig. 3(c), evidenced the rectangular and rod-like shapes of the alumina nanoparticles. Fig. 3(c) reveals the FESEM image of the sample after one hour of sonication, explaining a better dispersion. Another observation is that all the nanoparticles show a homogenous size distribution of $< 50$ nm. From Fig. 3(c), it could be inferred that the prepared nanoparticles are spherical with a full-size distribution based on the treatment. FESEM techniques can also measure the content of particles via the transmitted beam spectrum. This approach allows the differentiation of irregularly sized $Al_2O_3$ particles or any form of impurity; it can also help in confirming the surface distribution of $Al_2O_3$ nanoparticles on the sample. Fig. 3(c) also suggests that $Al_2O_3$ accounted for the more substantial bulk of the sample, thereby confirming its high purity and approving the adopted synthesis method. When synthesizing the nanofluids, no surfactants were used to guarantee higher thermal conductivity.

The FESEM image of $SiO_2$-$H_2O$ nanofluid, as shown in Fig. 3(d), indicated the round and rod-like shape of the silica nanoparticles. The nanoparticles were also observed to be uniform and below 50 nm in size. The image of the sample after one-hour sonication is shown in Fig. 3(d), where the samples exhibited better dispersion compared to the non-sonicated samples. No surfactants were used to achieve more excellent thermal conductivities. Fig. 3(c–d) confirms that $SiO_2$ and $Al_2O_3$ accounted for most of the sample surface, signifying good sample quality, and validating the synthesis technique.

### 3.2. Analysis of thermal efficiency of flat-plate solar collector

The efficiency of the FPSC was evaluated using various types of nanofluids (GNPs, Gr, $Al_2O_3$ and $SiO_2$) at different concentrations by volume (0.25, 0.5, 0.75, and 1%), fluid inlet temperatures (30, 40, and 50 °C), mass flow rates (0.0085, 0.017, and 0.0255 kg/s) and heat supply rates (500, 750, and 1000 W/$m^2$). The efficiency ($\eta$) is plotted against the reduced temperature parameter (($T_{in}$-$T_a$)/$G_T$). Figs. 4–7 show the efficiency comparison of the solar collector for the base fluid (DW) and four types of nanofluids at different volume concentrations. The increments in the solar energy of using 0.25%-, 0.5%-, 0.75%- and 1%-$SiO_2$ were 1.34%, 2.63%, 3.93% and 4.09%, respectively. The increments in the solar energy of using 0.25%-, 0.5%-, 0.75%- and 1%-$Al_2O_3$ were 2.76%, 7.45%, 8.1% and 8.26%, respectively. While, the carbon base nanofluids (GNPs and Gr) show higher increments in the solar collector

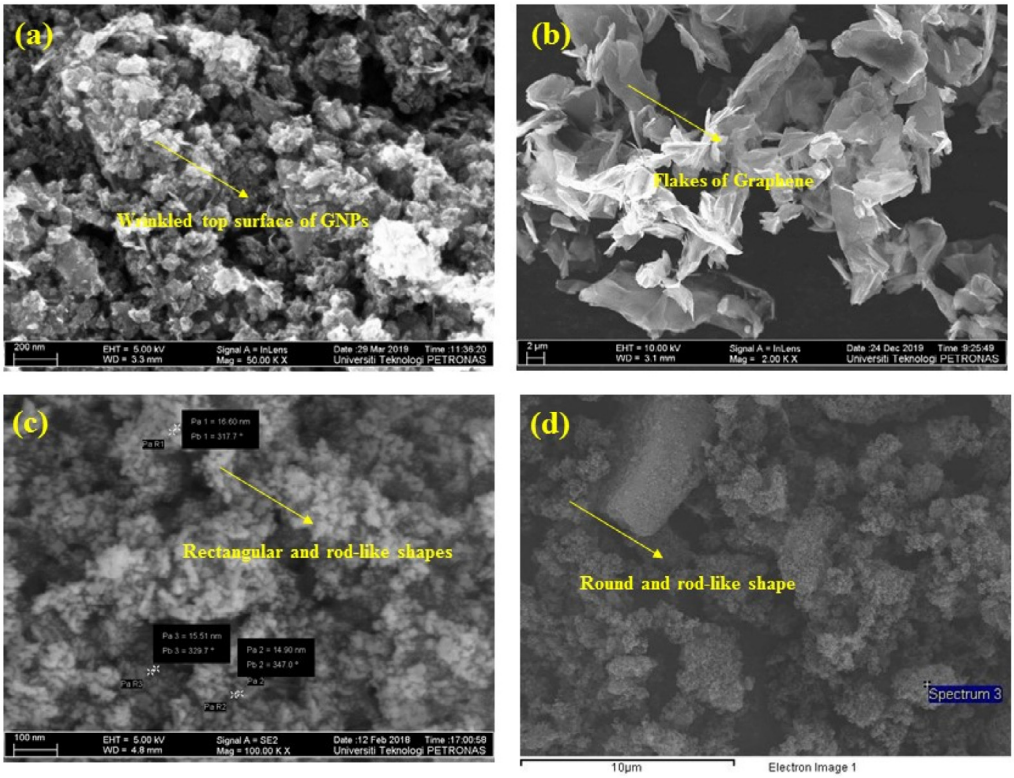


**Fig. 3.** FESEM images of different nanoparticles; (a) GNPs, (b) Gr, (c) $Al_2O_3$-NPs, (d) $SiO_2$-NPs.

efficiency as in the following: the increments in the recollected solar energy by using 0.25%-, 0.5%-, 0.75%- and 1%-Gr were 7.46%, 14.09%, 16.84%, and 17%, respectively. The increments in the solar energy of using 0.25%-, 0.5%-, 0.75%- and 1%-GNPs were 8.76%, 18.79%, 23.32% and 32.64%, respectively.

Figs. 4–7 show increases in the efficiency of the solar collector as a result of the introduction of the nanofluids as the base fluid. The introduction of the nanotubes improved the heat transfer between the solar collector and the base fluid, thereby enhancing the absorptivity and thermal conductivity of the base fluid. The different nanofluid types (GNPs, Gr, $Al_2O_3$, and $SiO_2$) significantly improved the efficiency of the system even at small concentrations (0.25, 0.5, 0.75, and 1%) (Karami et al., 2014; Eltaweel and Abdel-Rehim, 2019).

The intercept and slope of efficiency curve defined by collected data correspond to $F_R(\tau\alpha)$ and $F_RU_L$, absorbed energy coefficient and heat loss coefficient, respectively. $F_R(\tau\alpha)$ is the absorbed energy by the plate, while $F_RU_L$ is the heat loss to the surrounding. The two parameters have a significant impact on the solar collector's performance. The values of $F_R(\tau\alpha)$ and $F_RU_L$ are displayed in Tables 3–6. By increasing the volume fractions of the nanofluids, the absorbed energy parameter increased about (1.34%, 2.63%, 3.93% and 4.09%) for silica, (2.76%, 7.45%, 8.10% and 8.26%) for alumina, (7.46%, 14.09%, 16.84% and 17%) for graphene and (8.76%, 18.79%, 23.32% and 23.64%) for graphene nanoplatelets. The value of $F_RU_L$ for distilled water increased by (1.34%, 2.63%, 3.93% and 4.09%) for silica, (2.76%, 7.45%, 8.10% and 8.26%) for alumina, (7.46%, 14.09%, 16.84% and 17%) for graphene, and (8.76%, 18.79%, 23.32% and 23.64%) for graphene nanoplatelets. The incorporation of nanoparticles increased the outlet temperatures, i.e., more heat transmitted to the liquid, resulting in lower surface temperature resulting in lower energy loss.

**Table 3**
Heat gain and heat loss coefficients of $SiO_2$nanofluids at different mass flow rates.

| Heat gain coefficient ($F_R(\tau\alpha)$) | | | | | |
|---|---|---|---|---|---|
| Mass flow rate (kg/s) | DW | 0.25% $SiO_2$ | 0.5% $SiO_2$ | 0.75% $SiO_2$ | 1% $SiO_2$ |
| 0.0085 | 0.613 | 0.622 | 0.630 | 0.638 | 0.639 |
| 0.017 | 0.623 | 0.631 | 0.639 | 0.647 | 0.648 |
| 0.0255 | 0.626 | 0.634 | 0.642 | 0.650 | 0.651 |
| Heat loss coefficient ($F_RU_L$) | | | | | |
| Mass flow rate (kg/s) | DW | 0.25% $SiO_2$ | 0.5% $SiO_2$ | 0.75% $SiO_2$ | 1% $SiO_2$ |
| 0.0085 | 5.339 | 5.411 | 5.479 | 5.549 | 5.557 |
| 0.017 | 5.418 | 5.491 | 5.560 | 5.631 | 5.639 |
| 0.0255 | 5.441 | 5.514 | 5.584 | 5.655 | 5.663 |

## 4. Conclusions

The thermal efficiency of an FPSC utilizing distilled water, $SiO_2$, $Al_2O_3$, graphene, and graphene nanoplatelets as working fluids has been studied both experimentally and theoretically. Specific parameters such as different volume concentrations, different mass flow rates, different working fluid inlet temperatures and different values of solar irradiance have been checked. Added nanofluids of metallic oxides showed better thermal efficiency compared with the base liquid (water), while nanofluids based on carbon showed a further enhancement compared to metallic oxides. Increases in solar energy were 1.34%, 2.63%, 3.93% and 4.09%, respectively using 0.25%-, 0.5%-, 0.75%- and 1%-$SiO_2$. The rises in the use of solar energy of 0.25%, 0.5%, 0.75%, and 1%-$Al_2O_3$ were 2.76%, 7.45%, 8.1%, and 8.26%, respectively. While

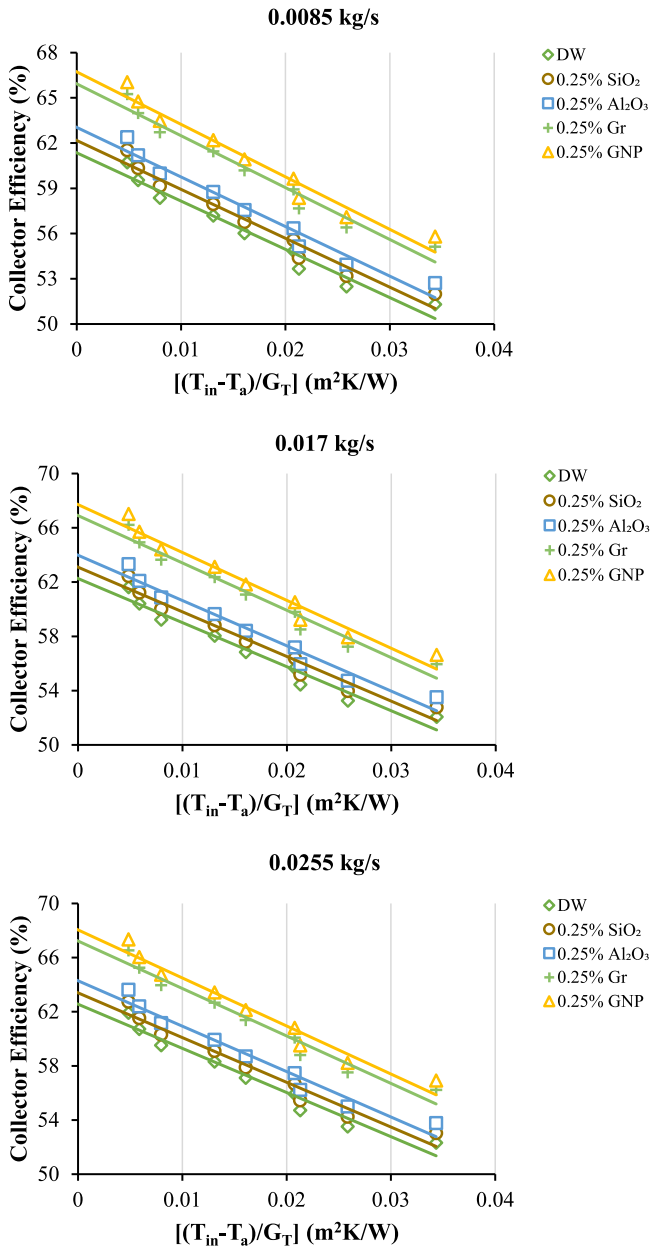


**Fig. 4.** Collector efficiency of different nanofluids at 0.25 vol.% for various mass flow rates.

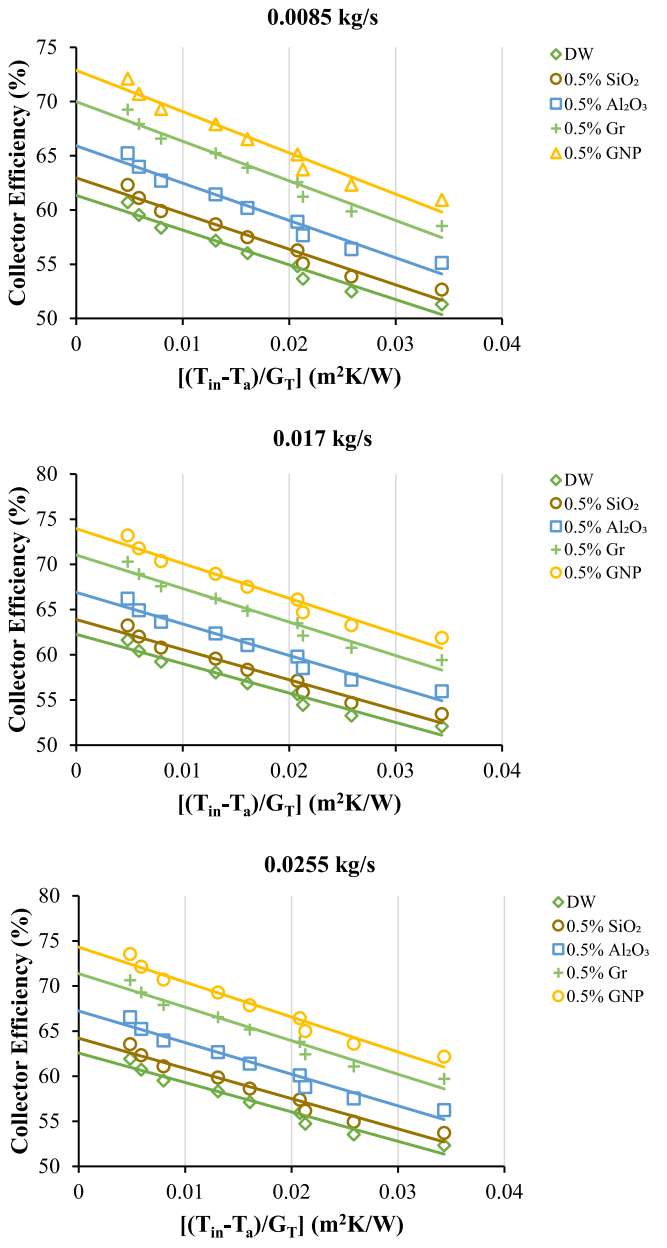


**Fig. 5.** Collector efficiency of different nanofluids at 0.5 vol.% for various mass flow rates.

**Table 4**
Heat gain and heat loss coefficients of $Al_2O_3$nanofluids at different mass flow rates.

| Heat gain coefficient ($F_R(\tau\alpha)$) | | | | | |
|---|---|---|---|---|---|
| Mass flow rate (kg/s) | DW | 0.25% $Al_2O_3$ | 0.5% $Al_2O_3$ | 0.75% $Al_2O_3$ | 1% $Al_2O_3$ |
| 0.0085 | 0.613 | 0.630 | 0.659 | 0.663 | 0.664 |
| 0.017 | 0.623 | 0.640 | 0.669 | 0.673 | 0.674 |
| 0.0255 | 0.626 | 0.643 | 0.672 | 0.676 | 0.677 |
| Heat loss coefficient ($F_RU_L$) | | | | | |
| Mass flow rate (kg/s) | DW | 0.25% $Al_2O_3$ | 0.5% $Al_2O_3$ | 0.75% $Al_2O_3$ | 1% $Al_2O_3$ |
| 0.0085 | 5.339 | 5.487 | 5.737 | 5.772 | 5.780 |
| 0.017 | 5.418 | 5.567 | 5.822 | 5.857 | 5.865 |
| 0.0255 | 5.441 | 5.591 | 5.846 | 5.881 | 5.890 |

**Table 5**
Heat gain and heat loss coefficients of graphene nanofluids at different mass flow rates.

| Heat gain coefficient ($F_R(\tau\alpha)$) | | | | | |
|---|---|---|---|---|---|
| Mass flow rate (kg/s) | DW | 0.25% Gr | 0.5% Gr | 0.75% Gr | 1% Gr |
| 0.0085 | 0.613 | 0.659 | 0.700 | 0.717 | 0.718 |
| 0.017 | 0.623 | 0.669 | 0.710 | 0.727 | 0.728 |
| 0.0255 | 0.626 | 0.672 | 0.714 | 0.731 | 0.732 |
| Heat loss coefficient ($F_RU_L$) | | | | | |
| Mass flow rate (kg/s) | DW | 0.25% Gr | 0.5% Gr | 0.75% Gr | 1% Gr |
| 0.0085 | 5.339 | 5.737 | 6.091 | 6.238 | 6.247 |
| 0.017 | 5.418 | 5.822 | 6.181 | 6.330 | 6.339 |
| 0.0255 | 5.441 | 5.847 | 6.207 | 6.357 | 6.366 |

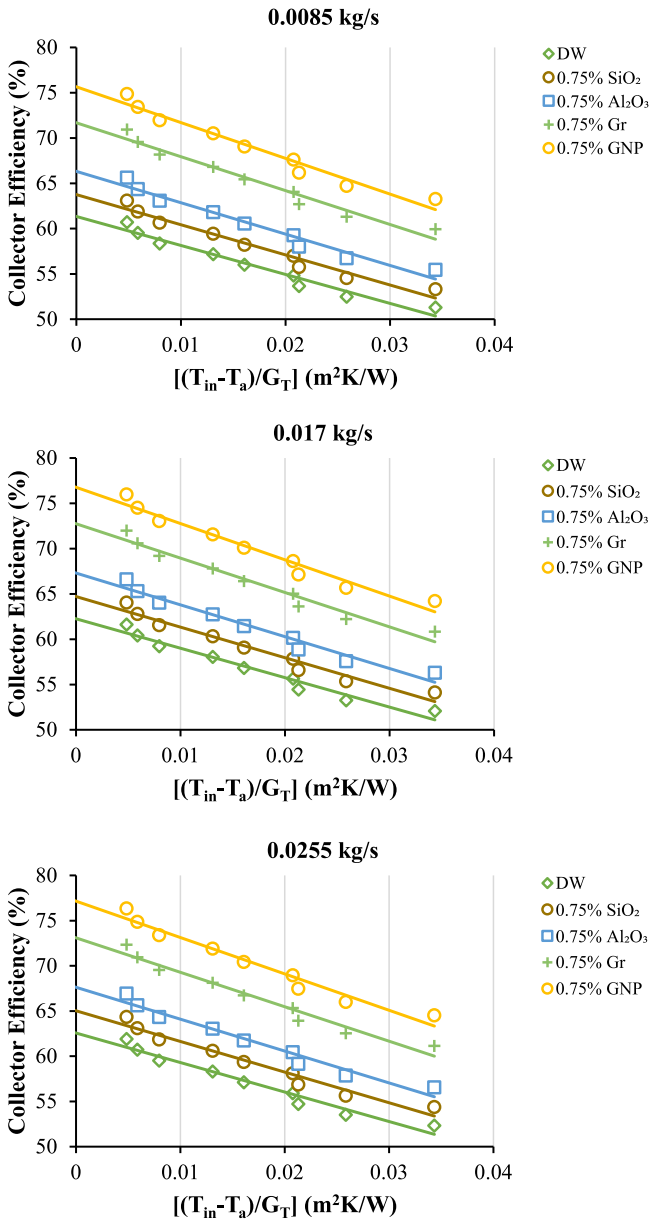


**Fig. 6.** Collector efficiency of different nanofluids at 0.75 vol.% for various mass flow rates.

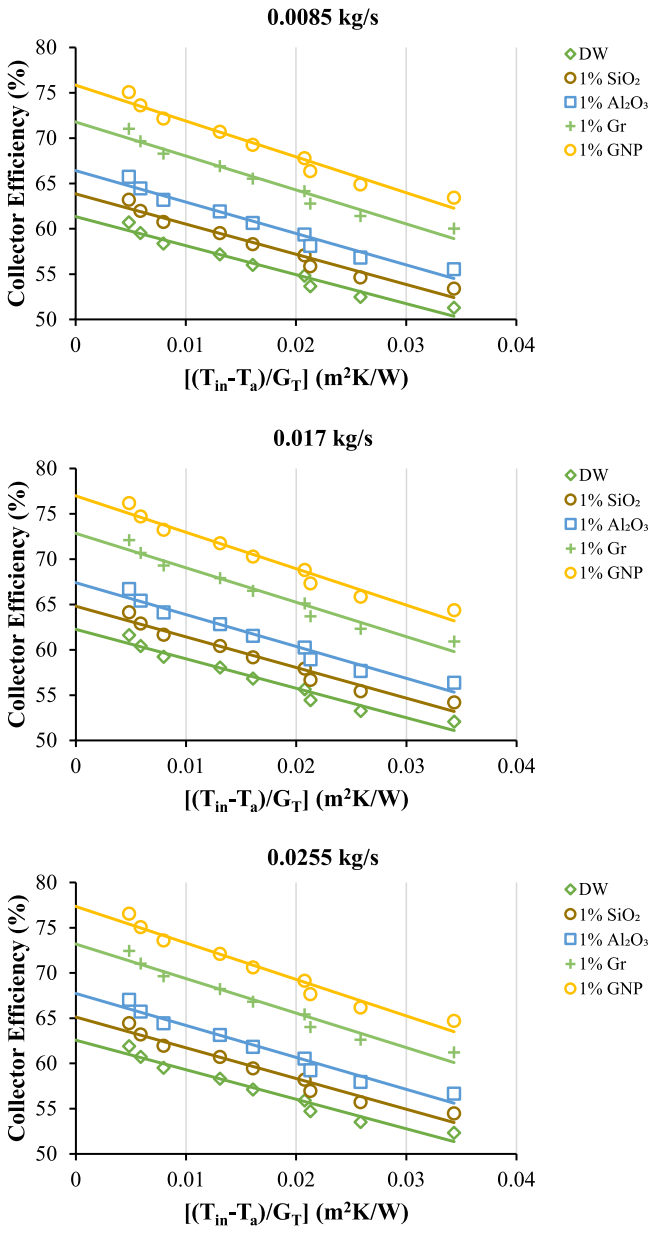


**Fig. 7.** Collector efficiency of different nanofluids at 1 vol.% for various mass flow rates.

**Table 6**
Heat gain and heat loss coefficients of graphene nanoplatelets nanofluids at different mass flow rates.

| Heat gain coefficient ($F_R(\tau\alpha)$) | | | | | |
|---|---|---|---|---|---|
| Mass flow rate (kg/s) | DW | 0.25% GNP | 0.5% GNP | 0.75% GNP | 1% GNP |
| 0.0085 | 0.613 | 0.667 | 0.729 | 0.757 | 0.758 |
| 0.017 | 0.623 | 0.677 | 0.740 | 0.768 | 0.770 |
| 0.0255 | 0.626 | 0.680 | 0.743 | 0.772 | 0.774 |
| Heat loss coefficient ($F_RU_L$) | | | | | |
| Mass flow rate (kg/s) | DW | 0.25% GNP | 0.5% GNP | 0.75% GNP | 1% GNP |
| 0.0085 | 5.339 | 5.807 | 6.342 | 6.584 | 6.601 |
| 0.017 | 5.418 | 5.892 | 6.436 | 6.681 | 6.699 |
| 0.0255 | 5.441 | 5.918 | 6.463 | 6.710 | 6.727 |

the carbon-based nanofluids (GNPs and Gr) showed greater improvements in solar collector performance as follows; rises in solar energy use of 0.25%-, 0.5%-, 0.75%-and 1%-Gr were 7.46%, 14.09%, 16.84%, and 17% respectively. Increases in solar energy were 8.76%, 18.79%, 23.32% and 32.64%, respectively of using 0.25%, 0.5%, 0.75%, and 1% of GNPs. Upon increasing the volume fractions of the nanofluids, the absorbed energy parameter increased approximately (1.34%, 2.63%, 3.93% and 4.09%) for $SiO_2$, (2.76%, 7.45%, 8.10% and 8.26%) for $Al_2O_3$, (7.46%, 14.09%, 16.84% and 17%) for Gr, and (8.76%, 18.79%, 23.32% and 23.64%) for GNPs. The value of FRUL with respect to distilled water was increased (1.34%, 2.63%, 3.93% and 4.09%) for $SiO_2$, (2.76%, 7.45%, 8.10% and 8.26%) for $Al_2O_3$, (7.46%, 14.09%, 16.84% and 17%) for Gr, and (8.76%, 18.79%, 23.32% and 23.64%) for GNPs (see Table 7).

**Table 7**

| | | | |
|---|---|---|---|
| **Nomenclature** | | | |
| $A_c$ | Surface area of the solar collector ($m^2$) | *GNPs* | Graphene Nanoplatelets |
| $Al_2O_3$ | Aluminum oxide | *GO* | Graphene oxide |
| $C_b$ | Tube-plate bond conductance (W/m K) | *Gr* | Graphene |
| $C_p$ | Specific heat capacity (kJ/kg K) | $G_T$ | Global solar radiation ($W/m^2$) |
| CuO | Copper oxide | $k$ | Thermal conductivity (W/m K) |
| $D$ | Tube diameter (m) | $L$ | Characteristic length (m) |
| $D_i$ | Inner tube diameter (m) | *MWCNTs* | Multi-Walled Carbon Nanotubes |
| *DSC* | Differential *scanning calorimeter* | $\dot{m}$ | Mass flow rate (kg/s) |
| $F$ | Standard fin efficiency | $Q_{loss}$ | Overall heat loss (W) |
| $F'$ | Collector efficiency factor | $SiO_2$ | Silicon dioxide |
| $F''$ | Collector flow factor | *SWCNT* | Single-Wall Carbon Nanotubes |
| *FESEM* | Field Emission Scanning Electron Microscopy | $T_a$ | Temperature (K) |
| *FPSC* | Flat plate solar collector | $TiO_2$ | Titanium oxide |
| $F_R$ | Heat removal factor | $U_L$ | Overall heat losses coefficient ($W/m^2$ K) |
| $F_R(\tau\alpha)$ | Heat absorbed coefficient | $U_t$ | Top loss coefficient ($W/m^2$ K) |
| $F_RU_L$ | Heat removed coefficient | $W$ | Space between two parallel tubes |
| **Greek symbols** | | | |
| $\gamma$ | The average bond thickness | $\rho$ | Density of fluid ($kg/m^3$) |
| $\eta_{th}$ | Thermal efficiency of FPSC | $\phi$ | Volume concentration (vol.%.) |
| **Subscripts** | | | |
| $a$ | Ambient | $nf$ | Nanofluids |
| $b$ | Back of the collector | $np$ | Nanoparticles |
| $bf$ | Base fluid | $o$ | Outlet |
| $e$ | Edge of the collector | $pm$ | Plate mean temperature |
| $i$ | Inlet | $t$ | Top |

## CRediT authorship contribution statement

**Suhong Liu:** Formal analysis, Funding acquisition, Writing - original draft, Writing - review & editing. **Haitham Abdulmohsin Afan:** Formal analysis, Project administration, Software, Writing - original draft, Writing - review & editing. **Mohammed Suleman Aldlemy:** Formal analysis, Investigation, Validation, Visualization, Writing - original draft. **Nadhir Al-Ansari:** Funding acquisition, Supervision, Writing - original draft, Writing - review & editing. **Zaher Mundher Yaseen:** Conceptualization, Formal analysis, Investigation, Resources, Supervision, Writing - original draft.

## Declaration of competing interest

The authors declare that they have no known competing financial interests or personal relationships that could have appeared to influence the work reported in this paper.

## Acknowledgments

The research was supported by the Key Research and Development Program in Shaanxi Province under Grant. 2016GY-083. The authors appreciate the experimental laboratory support provided by the Universiti Teknologi Petronas. Further, we do thank the respected editors and reviewers for their excellent comments to enhance the visualization of the presented research.

## References

Ahmadi, A., Ganji, D.D., Jafarkazemi, F., 2016. Analysis of utilizing graphene nanoplatelets to enhance thermal performance of flat plate solar collectors. Energy Convers. Manage. 126, 1–11. http://dx.doi.org/10.1016/j.enconman.2016.07.061.

Akram, N., Sadri, R., Kazi, S.N., Ahmed, S.M., Zubir, M.N.M., Ridha, M., Soudagar, M., Ahmed, W., Arzpeyma, M., Tong, G.B., 2019. An experimental investigation on the performance of a flat-plate solar collector using eco-friendly treated graphene nanoplatelets–water nanofluids. J. Therm. Anal. Calorim. 138, 609–621. http://dx.doi.org/10.1007/s10973-019-08153-4.

Alawi, O.A., Mallah, A.R., Kazi, S.N., Sidik, N.A.C., Najafi, G., 2019a. Thermophysical properties and stability of carbon nanostructures and metallic oxides nanofluids. J. Therm. Anal. Calorim. 135, 1545–1562. http://dx.doi.org/10.1007/s10973-018-7713-x.

Alawi, O.A., Mohamed Kamar, H., Mallah, A.R., Kazi, S.N., Sidik, N.A.C., 2019b. Thermal efficiency of a flat-plate solar collector filled with Pentaethylene Glycol-Treated Graphene Nanoplatelets: An experimental analysis. Sol. Energy 191, 360–370. http://dx.doi.org/10.1016/j.solener.2019.09.011.

Alawi, O.A., Sidik, N.A.C., Kazi, S.N., Najafi, G., 2019c. Graphene nanoplatelets and few-layer graphene studies in thermo-physical properties and particle characterization. J. Therm. Anal. Calorim. 135, 1081–1093. http://dx.doi.org/10.1007/s10973-018-7585-0.

Alim, M.A., Abdin, Z., Saidur, R., Hepbasli, A., Khairul, M.A., Rahim, N.A., 2013. Analyses of entropy generation and pressure drop for a conventional flat plate solar collector using different types of metal oxide nanofluids. Energy Build. 66, 289–296. http://dx.doi.org/10.1016/j.enbuild.2013.07.027.

Amin, T.E., Roghayeh, G., Fatemeh, R., Fatollah, P., 2015. Evaluation of nanoparticle shape effect on a nanofluid based flat-plate solar collector efficiency. Energy Explor. Exploit. 33, 659–676. http://dx.doi.org/10.1260/0144-5987.33.5.659.

Azmi, W.H., Sharma, K.V., Mamat, R., Najafi, G., Mohamad, M.S., 2016. The enhancement of effective thermal conductivity and effective dynamic viscosity of nanofluids – A review. Renew. Sustain. Energy Rev. 53, 1046–1058. http://dx.doi.org/10.1016/j.rser.2015.09.081.

Borode, A., Ahmed, N., Olubambi, P., 2019. A review of solar collectors using carbon-based nanofluids. J. Cleaner Prod. http://dx.doi.org/10.1016/j.jclepro.2019.118311.

Choi, S.U.S., Eastman, J.A., 1995. Enhancing thermal conductivity of fluids with nanoparticles. ASME Int. Mech. Eng. Congr. Exp. 66, 99–105. http://dx.doi.org/10.1115/1.1532008.

Duffie, J.A., Beckman, W.A., 2013. Solar Engineering of Thermal Processes. John Wiley & Sons.

Eltaweel, M., Abdel-Rehim, A.A., 2019. Energy and exergy analysis of a thermosiphon and forced-circulation flat-plate solar collector using MWCNT/Water nanofluid. Case Stud. Therm. Eng.

Faizal, M., Saidur, R., Mekhilef, S., Alim, M.A., 2013. Energy, economic and environmental analysis of metal oxides nanofluid for flat-plate solar collector. Energy Convers. Manage. 76, 162–168. http://dx.doi.org/10.1016/j.enconman.2013.07.038.

Farhana, K., Kadirgama, K., Rahman, M.M., Ramasamy, D., Noor, M.M., Najafi, G., Samykano, M., Mahamude, A.S.F., 2019. Improvement in the performance of solar collectors with nanofluids — A state-of-the-art review. Nano-Struct. Nano-Objects 18, 100276. http://dx.doi.org/10.1016/j.nanoso.2019.100276.

Gupta, M., Singh, V., Kumar, R., Said, Z., 2017. A review on thermophysical properties of nanofluids and heat transfer applications. Renew. Sustain. Energy Rev. 74, 638–670. http://dx.doi.org/10.1016/j.rser.2017.02.073.

Hajabdollahi, Z., Hajabdollahi, H., Kim, K.C., 2019. Multi-objective optimization of solar collector using water-based nanofluids with different types of nanoparticles. J. Therm. Anal. Calorim. 1–12, in press.

Kabeel, A.E., Khalil, A., Shalaby, S.M., Zayed, M.E., 2016. Investigation of the thermal performances of flat, finned, and v-corrugated plate solar air heaters. J. Sol. Energy Eng. 138, 51004.

Kalogirou, S.A., 2013. Summary for Policymakers. In: Intergovernmental Panel on Climate Change (Ed.), Climate Change 2013 - the Physical Science Basis. Cambridge University Press, Cambridge, pp. 1–30. http://dx.doi.org/10.1017/CBO9781107415324.004.

Karami, M., Akhavan Bahabadi, M.A., Delfani, S., Ghozatloo, A., 2014. A new application of carbon nanotubes nanofluid as working fluid of low-temperature direct absorption solar collector. Sol. Energy Mater. Sol. Cells 121, 114–118.

Kong, W., Perers, B., Fan, J., Furbo, S., Bava, F., 2015. A new Laplace transformation method for dynamic testing of solar collectors. Renew. Energy 75, 448–458.

Li, S., Wang, H., Meng, X., Wei, X., 2017. Comparative study on the performance of a new solar air collector with different surface shapes. Appl. Therm. Eng. 114, 639–644.

Mahian, O., Kianifar, A., Sahin, A.Z., Wongwises, S., 2014. Performance analysis of a minichannel-based solar collector using different nanofluids. Energy Convers. Manage. 88, 129–138. http://dx.doi.org/10.1016/j.enconman.2014.08.021.

Mallah, A.R., Mohd Zubir, M.N., Alawi, O.A., Salim Newaz, K.M., Mohamad Badry, A.B., 2019. Plasmonic nanofluids for high photothermal conversion efficiency in direct absorption solar collectors: Fundamentals and applications. Sol. Energy Mater. Sol. Cells 201, 110084. http://dx.doi.org/10.1016/j.solmat.2019.110084.

Pak, B.C., Cho, Y.I., 1998. Hydrodynamic and heat transfer study of dispersed fluids with submicron metallic oxide particles. Exp. Heat Transfer 11, 151–170. http://dx.doi.org/10.1080/08916159808946559.

Raj, P., Subudhi, S., 2018. A review of studies using nanofluids in flat-plate and direct absorption solar collectors. Renew. Sustain. Energy Rev. 84, 54–74. http://dx.doi.org/10.1016/j.rser.2017.10.012.

Sadripour, S., 2017. First and second laws analysis and optimization of a solar absorber; using insulator mixers and MWCNTs nanoparticles. Global J. Res. Eng..

Said, Z., Saidur, R., Rahim, N.A., Alim, M.A., 2014. Analyses of exergy efficiency and pumping power for a conventional flat plate solar collector using SWCNTs based nanofluid. Energy Build. 78, 1–9. http://dx.doi.org/10.1016/j.enbuild.2014.03.061.

Said, Z., Saidur, R., Sabiha, M.A., Rahim, N.A., Anisur, M.R., 2015. Thermophysical properties of Single Wall Carbon Nanotubes and its effect on exergy efficiency of a flat plate solar collector. Sol. Energy 115, 757–769. http://dx.doi.org/10.1016/j.solener.2015.02.037.

Sarsam, W.S., Kazi, S.N., Badarudin, A., 2015. A review of studies on using nanofluids in flat-plate solar collectors. Sol. Energy 122, 1245–1265. http://dx.doi.org/10.1016/j.solener.2015.10.032.

Sundar, L.S., Sharma, K.V., 2008. Thermal conductivity enhancement of nanoparticles in distilled water. Int. J. Nanoparticles 1, 66–77.

Tong, YijieLee, H., Kang, W., Cho, H., 2019. Energy and exergy comparison of a flat-plate solar collector using water, Al2O3 nanofluid, and CuO nanofluid. Appl. Therm. Eng. 159, 113959. http://dx.doi.org/10.1016/j.applthermaleng.2019.113959.

Vakili, M., Hosseinalipour, S.M., Delfani, S., Khosrojerdi, S., Karami, M., 2016. Experimental investigation of graphene nanoplatelets nanofluid-based volumetric solar collector for domestic hot water systems. Sol. Energy 131, 119–130. http://dx.doi.org/10.1016/j.solener.2016.02.034.

Verma, S.K., Tiwari, A.K., Chauhan, D.S., 2017. Experimental evaluation of flat plate solar collector using nanofluids. Energy Convers. Manage. 134, 103–115. http://dx.doi.org/10.1016/j.enconman.2016.12.037.

Vincely, D.A., Natarajan, E., 2016. Experimental investigation of the solar FPC performance using graphene oxide nanofluid under forced circulation. Energy Convers. Manage. 117, 1–11.

Yousefi, T., Veisy, F., Shojaeizadeh, E., Zinadini, S., 2012. An experimental investigation on the effect of MWCNT-H2O nanofluid on the efficiency of flat-plate solar collectors. Exp. Therm Fluid Sci. 39, 207–212. http://dx.doi.org/10.1016/j.expthermflusci.2012.01.025.

Zayed, M.E., Zhao, J., Du, Y., Kabeel, A.E., Shalaby, S.M., 2019. Factors affecting the thermal performance of the flat plate solar collector using nanofluids: A review. Sol. Energy 182, 382–396. http://dx.doi.org/10.1016/j.solener.2019.02.054.